Transactions, SMiRT-26
Berlin/Potsdam, Germany, July 10-15, 2022
Division V

LOADING TESTS AND SEISMIC ANALYSIS FOR SHEAR WALL COMPOSED OF ULTRA-HIGH-PERFORMANCE-CONCRETE

Masaki Yukawa[1], Shinji Takami[2], Yoshitaka Takeuchi[3], Koichi Yabuuchi[4], Kentaro Mori[5], Yasuyoshi Nakayama[6], and Ritsu Hagiwara[7]

[1] Sub Manager, Obayashi Corporation, Tokyo, Japan (yukawa.masaki@obayashi.co.jp)
[2] Sub Director, Obayashi Corporation, Tokyo, Japan
[3] Senior Engineer, Obayashi Corporation, Tokyo, Japan
[4] Senior Manager, Kajima Corporation, Tokyo, Japan
[5] Senior Engineer, Mitsubishi Heavy Industries, Ltd., Hyogo, Japan
[6] Engineer, Hitachi-GE Nuclear Energy, Ltd., Ibaraki, Japan
[7] Deputy Manager, Toshiba Energy Systems & Solutions Corporation, Kanagawa, Japan

ABSTRACT

For the purpose of application of high-performance concrete to reactor buildings, in-plane loading test for shear walls using high-performance concrete was conducted. From the test results, τ-γ model and M-φ model applicable to high-performance concrete was proposed, and their applicability were confirmed consequently. In addition, seismic analysis was performed for PWR (Pressurized Water Reactor) building in each part of which high-performance concrete were applied, and the reduction of required wall thickness and improvement of seismic resistance performance due to higher material strength were confirmed. In conclusion, the effectiveness of application of high-performance concrete to reactor building was confirmed from these series of researches.

1. INTRODUCTION

Even though special concretes such as high-strength concrete, steel fiber-reinforced concrete and heavyweight concrete are not applied to structural walls of buildings in Japanese nuclear power plants, however, when used properly, their characteristics may enhance the performance of nuclear power plant buildings and equipment in terms of improvements of seismic response characteristics and may reduce the weight of upper structures . There isn't sufficient experimental data or knowledge on dynamic characteristics of high-performance concrete because of a lack of experimental study on shear walls using these materials. This paper shows the performance of horizontal loading tests of seismic resistance walls using the special concretes performed to identify their characteristics as well as to model their shear and bending restoring force characteristics. Furthermore, seismic response analyses of multiple lumped mass model using the restoring force characteristics was performed to clarify the validity of the building and reaction reduction effect.
This study had been carried out in the project "Development of technical infrastructure for upgrading materials, structures and construction methods of nuclear power plant buildings"

2. TEST SPECIMENS

Table 2.1 shows a list of specimens whose shapes are shown in Figure 2.1. Major parameters of the test are concrete strength, and types of fiber-reinforcements. The target of the tests is to obtain test data to be

used for setting parameters of τ-γ model and M-φ model; therefore, two test cases are planned; namely, "shear failure case" and "bending failure case." In order to control the failure mode, vertical axial force (axial stress of 0.095 times σ_B for whole section of a wall, where σ_B is compression strength) is applied in shear failure case, whereas no axial force is applied in bending failure case.
To intentionally controls the deformation mode, vertical loads to be 0.095times of concrete strength are applied to shear deformation tests. All specimens have a same shape (I-shape) where web wall thickness is 150mm, web wall length is 2000mm, flange wall width is 1000mm, and the shear span ratio (M/Qd) is 0.6. The reinforcement bars are SD490 (yield strength is 490N/mm^2), and the maximum aggregate size is 15mm. Simulating an actual structure condition, the boundary of top and bottom of the wall potion have joints where fiber-reinforcements cannot carry force cross the joints.

Table 2.1. A list of specimens

Number of test specimens	Test type	Concrete strength (N/mm^2)	Volume ratio of steel fiber (%/Vol.)	Volume ratio of organic fiber (%/Vol.)	Compression strength*1 (N/mm^2)	Tension split strength*1 (N/mm^2)
1	Shear load	Fc33	-	-	35.5	3.68
2		Fc150	-	-	184	5.65
3		Fc100 (with organic fiber)	-	0.22	163	7.90
4		Fc150 (with organic fiber and steel fiber)	1.0	0.11	188	7.68
5		Fc60 (heavy weight concrete)	-	-	80.8	4.72
6	Bending load	Fc150 (with organic fiber and steel fiber)	1.0	0.22	199	7.92

Fc : Design standard strength
*1 : In principle, obtained from the material test using test piece (100mm diameter, On-site seal curing) on the same day as the loading test

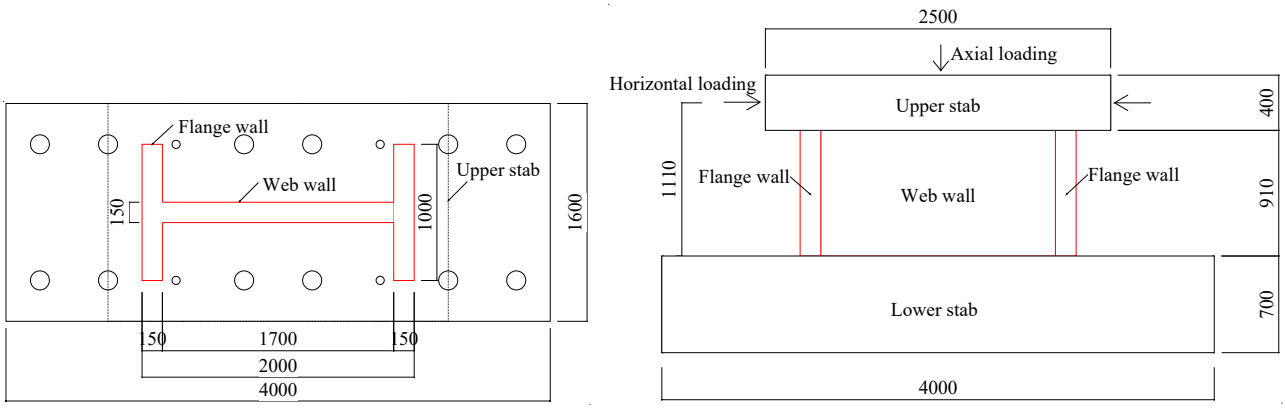

(a) Plan view (b) Elevation view

Figure 2.1. Test specimen shape

3. TEST CONDITION

Figure 3.1 shows the test equipment jig and Figure 3.2 shows the loading programs. The bottom of the lower stab is fixed to a reaction wall, and the horizontal force by hydraulic jack in positive and negative direction along with a constant vertical load is applied to the upper stab. To avoid a twist deformation, the

upper stab is supported by side guides to constrain the deformation in out-of-plane direction of the load. The loading is controlled by displacements where differences of upper stab to lower stab divided by the wall height is considered as the wall deformation angle. The program applies cyclic loading begins at ±0.5/1000radian to gradual increase (two cycles each) up to 80% reduction compared to the maximum reaction force is observed.

Figure 3.3 shows the test measurement system. Displacement meters are used to measure deformation of the specimens where shear deformation and bending deformation can be separately evaluated. Strain gauges are used to measure reinforcement bar strain to grasp the strain distributions and yield locations.

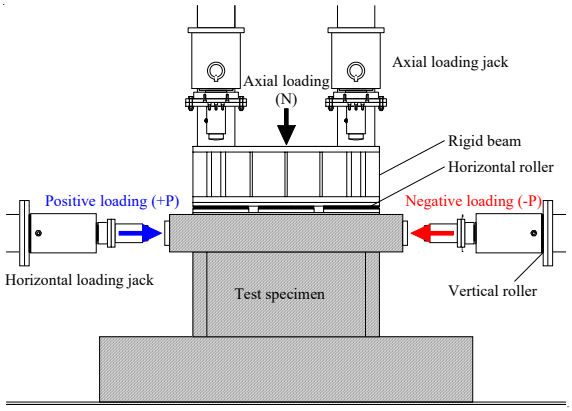

Figure 3.1. The overview of test setup

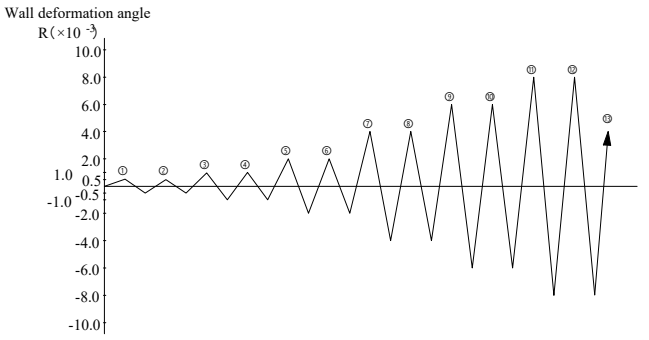

Figure 3.2. The loading program

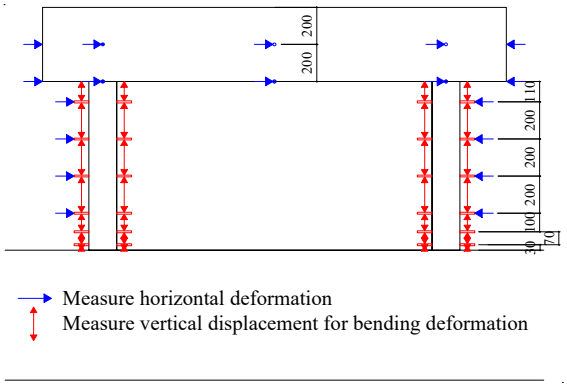

(a) Deformation measurement of test specimen

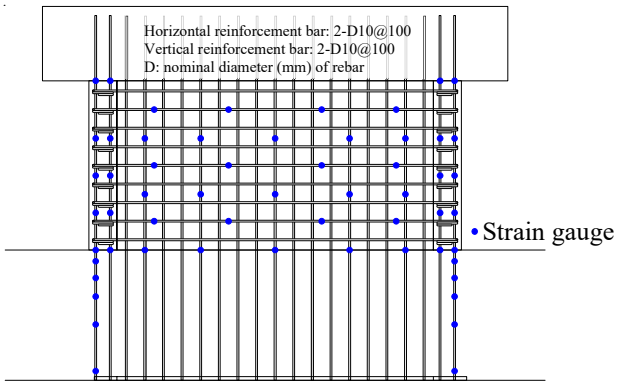

(b) Strain measurement of reinforcement bar

Figure 3.3. The test measurement system

4. TEST RESULTS

4.1 Failure Mode

Figure 4.1.1 shows the final conditions of test specimens. In the shear failure type specimens (No.1 to No.5), shear cracks on the web portion firstly appears followed by bending cracks on the flange portion; and vertical reinforcement bars of these specimens did not yield so that shear failure controlled these specimens as intended to do so. The other bending failure type specimen (No.6), on the contrary, bending cracks on the flange portion firstly appears followed by shear cracks on the web portion. Then, the vertical reinforcement bars in a flange wall in tension side and web wall yielded, which means bending failure; note that slip failure at the bottom of the wall is also appeared in No.6 specimen. Relatively low strength concrete specimens (No.1: Fc30 and No.5: heavy weight concrete) show moderate failure at the final stage,

but high strength concrete specimens (No.2: Fc150) shows aggressive failure with spalling at the final stage. Specimens No.3 (Fc100 with organic fiber) and No.4 (Fc150 with steel fiber) are also made of high strength concrete but because of fiber-reinforcement, its failure is less aggressive, especially specimen No.4 with steel type fiber-reinforcement is much less aggressive (similar to No.1) failure.

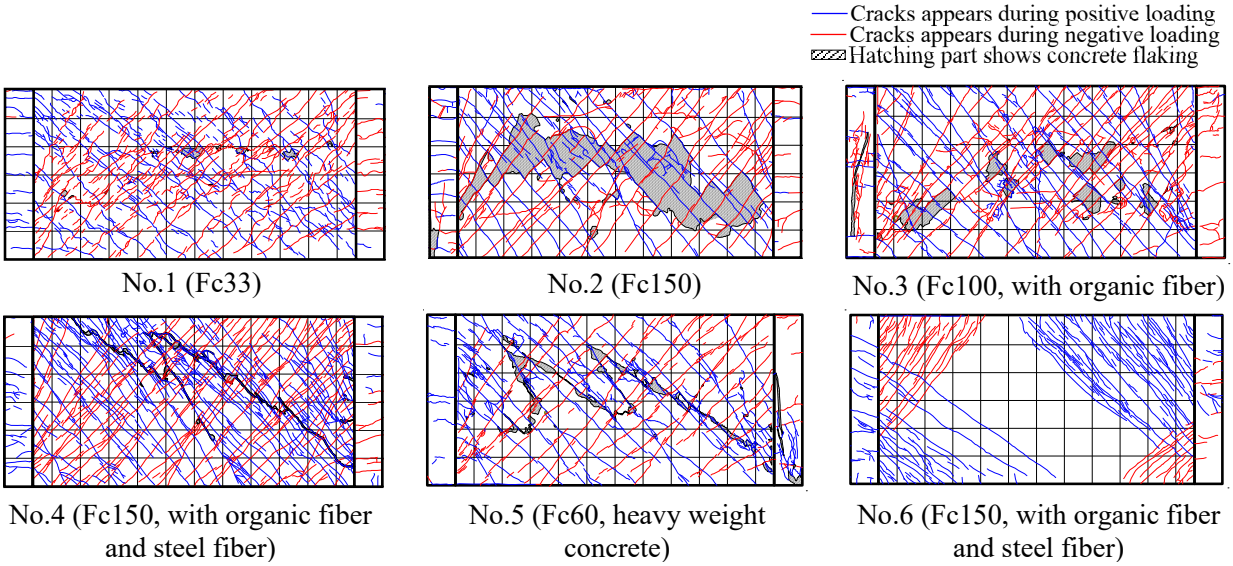

Figure 4.1.1. The final conditions of test specimens

4.2 Load- wall deformation angle relations

Figure 4.2.1 shows load-wall deformation angle relations of specimens and Figure 4.2.2 shows their skeleton curves. Note that the constant peak loads observed in specimen No.6 specimen is presumed to be caused by the slip of wall bottom during the test.

The maximum load of specimens No.2 and No.4 are 2.66 and 1.26 times that of No.1, respectively; the increase includes the increase of concrete strength due to the large vertical load applied, and besides, the major causes of this phenomena are confirmed to be the employment of high strength concrete or steel fiber-reinforcements. The deformation at the maximum load of specimen No.2 (Fc150) was less than that of specimen No.1 (Fc33). The maximum deformation angle of specimen No.2 was achieved at 7.57×10^{-3} radian, and the load level had not dropped until the deformation became relatively large enough. The maximum deformation angle of specimen No.4 (Fc150 with steel fiber) was achieved at 11.8×10^{-3} radian, which is larger than that of specimen No.2 (Fc150) due to the steel fiber-reinforcements. The relationship between load and displacement hysteresis for all the specimens (No.1 to No.5) shows origin-oriented type characteristics that is typical for shear failure type specimens.

The concrete strength of specimen No.3 (Fc100 with organic fiber) is less than that of specimen No.2 (Fc150) by 11 %. Nevertheless, these specimens show a similar strength and skeleton curve, whose reason is not clarified, but the spalling of cover concrete was prevented by the organic fiber to some extent, and thus the decrease of shear resistance due to the concrete fracture was also prevented.

Table 4.2.1 shows test results and Figure 4.2.3 shows comparison of maximum share strength of this tests and compressive strength of the concrete material tests. All shear test results showed maximum share strain capacity more than the design limit of Japanese design standard JEAC4601[1)] (4000μ). Strong positive correlation between concrete strength and shear strength of the wall is observed for the wall using concrete with wide range of strength up to Fc150.

Table 4.2.1. A list of test results

Spicemen	Load direction	Failure mode	Bending crack		Shear crack		Maximum strangth		
			Force (kN)	Deformatin angle ($\times 10^{-3}$rad)	Force (kN)	Deformatin angle ($\times 10^{-3}$rad)	Force (kN)	Deformatin angle ($\times 10^{-3}$rad)	Shear strain (μ)
No.1	positive (+)	Shear	+1222	+1.44	+821	+0.62	+2717	+9.72	+7930
	Negative (-)		-1163	-1.24	-730	-0.47	-2643	-8.00	-6480
No.2	positive (+)	Shear	+6327	+4.00	+2861	+0.8	+7236	+7.57	+6040
	Negative (-)		-6529	-4.00	-2892	-0.75	-7190	-6.00	-4900
No.3	positive (+)	Shear	+4785	+2.00	+2605	+0.75	+7105	+8.00	+5970
	Negative (-)		-4442	-1.76	-3044	-0.77	-6909	-6.01	-4780
No.4	positive (+)	Shear	+7452	+4.00	+3454	+0.93	+9099	+11.8	+8360
	Negative (-)		-7647	-4.00	-3190	-0.80	-8864	-8.00	-5760
No.5	positive (+)	Shear	+3051	+1.30	+2260	+0.75	+4802	+6.01	+4560
	Negative (-)		-3174	-1.40	-2354	-0.75	-4735	-6.01	-4610
No.6	positive (+)	Bending (sliding at joint)	+1071	+0.566	+1806	+1.3	+2465	+4.00	+1350
	Negative (-)		-2465	-4.00	-1836	-1.6	-2203	-4.00	-1250

The underline shows that cracks have already occurred when observing the cycle peak

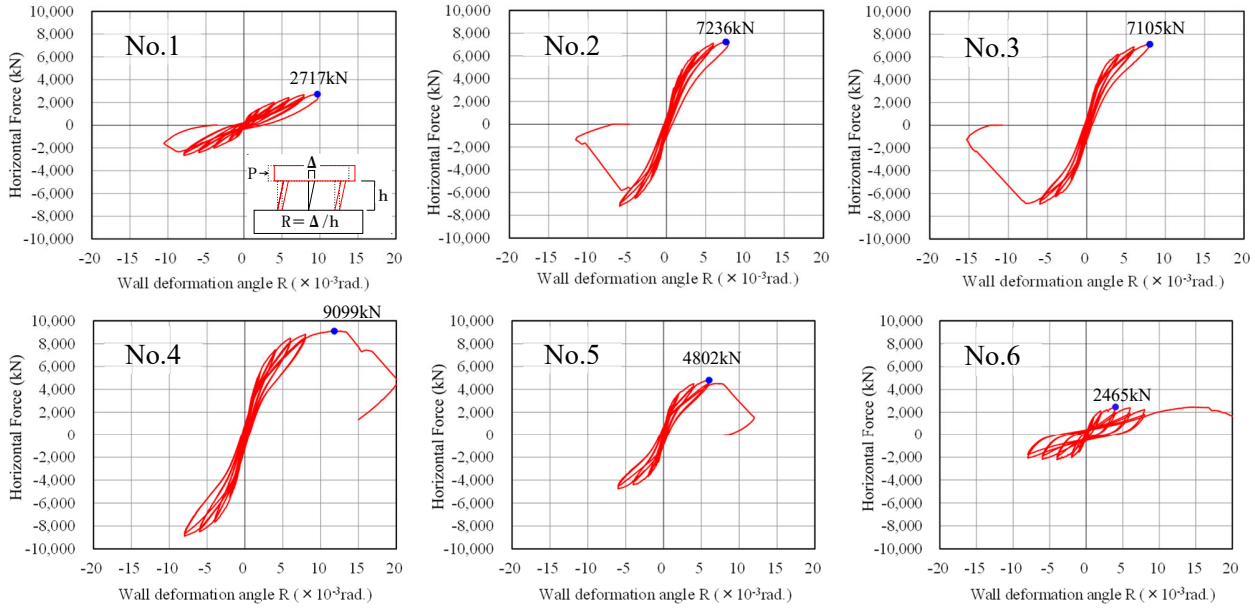

Figure 4.2.1. Load- wall deformation angle relations of specimens

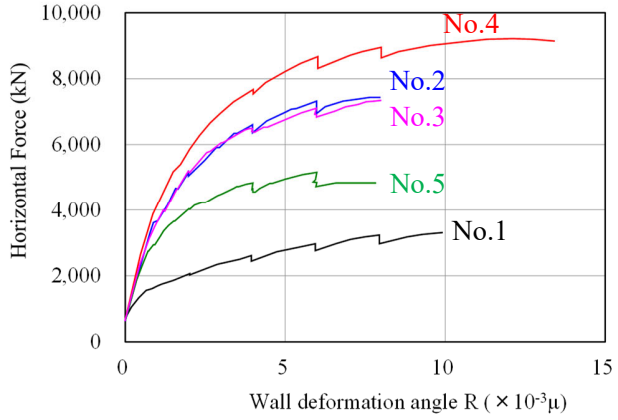

Figure 4.2.2. Skelton curves of specimens

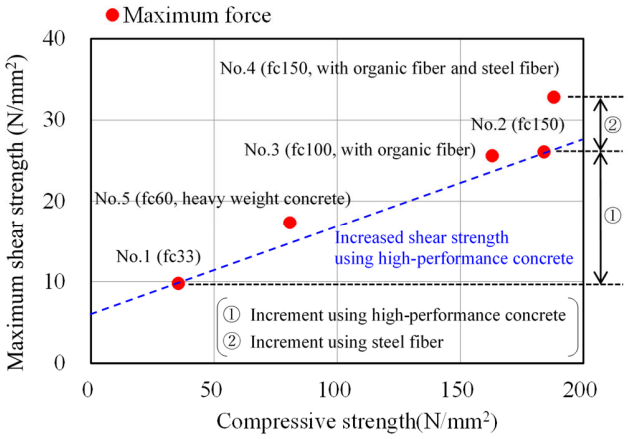

Figure 4.2.1. Relationship between maximum shear strength and compressive strength

4.3 Restoring characteristic models for design

(1) Shear stress-Shear strain (τ-γ) Model
For a shear stress-shear strain model, JEAC4601 is usually applied, but the compressive strength of high-performance concrete is larger than the scope of the standard, i.e. concrete strength equal to or less than 60 N/mm^2; therefore, in this study, based on the test results of high-strength concrete specimens, some of the JEAC4601 test parameters are updated as shown in Table 4.3.1.
In addition, tensile stress on concrete increased by the steel fiber-reinforcement effect (cross-linking effect) is also considered for steel fiber-reinforced concrete. An approximately 5.5N/mm^2 tensile stress (σ_t) is maintained with a crack width of up to 0.5mm when the amount of steel fiber-reinforcement is 1.0vol.%[2)]. The relation of the ultimate shear stain γ_w and the ultimate tensile strain ε_t of the wall is assumed to be explained by Equation 4.3.1. In specimen No.4 which contains steel fiber, the ultimate shear stain is 8,360μ and an average of crack intervals L_{cr} is less than 100mm. Thus, a crack width of 0.42mm which is less than 0.5mm is given from Equation 4.3.2 by γ_w= 8,360 and L_{cr}= 100, which means that the tensile stress of approximately 5.5 N/mm^2 is expected in this study[3)]. A concept image of in-plane stress after the development of cracks is shown in Figure 4.3.1. When the direction of main stress is assumed to be in 45 degrees at loading, the shear resistance of steel fiber-reinforcement can be expressed in Equation 4.3.3, which is then added to the ultimate shear stress used for the restoring force characteristics.
Figure 4.3.2 shows the comparison of proposed restoring force characteristics to the test results. Shear deformation component is calculated by subtracting bending component (given by the observed data from vertical displacement meters) from the total deformation. The proposed models for the specimen with high-performance concrete and with steel fiber-reinforcement showed larger strength than that of JEAC4601 design model, which means that the proposed model is in better accordance with the test results than JEAC4601 model.

$$\varepsilon_t \fallingdotseq \gamma_w/2 \tag{4.3.1}$$

$$W_{cr} = L_{cr} \times \varepsilon_t \tag{4.3.2}$$

$$\tau_{fib} = \sigma_t \times \sin\theta \times \cos\theta \tag{4.3.3}$$

Where, τ_{fib} is shear resistance of steel fiber-reinforcement, θ is the principal stress angle.

Table 4.3.1. The comparison restoring force characteristic of JEAC4601 and proposed model

		Shear stress at turning points (N/mm^2)		
		First	Second	Third
Sear stress equation		$\tau_1 = \sqrt{F_t(F_t + \sigma_v)}$ $F_t = 0.31\sqrt{F_c}$	$\tau_2 = \kappa \times \tau_1$	$\tau_s \le A \times F_C^B$ $\tau_3 = \{1 - \tau_s/(A \times F_C^B)\}\tau_0 + \tau_s$ $\tau_s \ge A \times F_C^B$ $\tau_3 = A \times F_C^B$
Coefficient	Fc≦60N/mm^2 *1	-	$\kappa = 1.35$	$A = 1.4\,, B = 0.5$
	Fc > 60N/mm^2 *2	-	$\kappa = 1.35 + (\sigma_B - 60)/250$	$A = 0.55\,, B = 0.8$

*1: Conventional parameters from JEAC4601, *2: Proposed parameters in this study
σ_B: Actual compressive stress (N/mm^2), σ_v: vertical axial stress, σ_h: Horizontal axial stress, P_v: Vertical steel reinforcement ratio, P_h: Horizontal steel reinforcement ratio, ${}_s\sigma_y$: yield stress of steel reinforcement
$\tau_0 = (0.67 - 0.4M/QD) \times A \times F_C^B$, $\tau_s = (P_V + P_H)\ {}_s\sigma_y/2 + (\sigma_V + \sigma_H)/2$

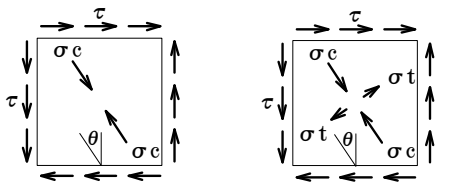

(a) No steel fiber (b) With steel fiber

σ_c : Compression stress of concrete
σ_t : Tensile stress of concrete

Figure4.3.1. The assumption of in-plane stress condition after the development of cracks

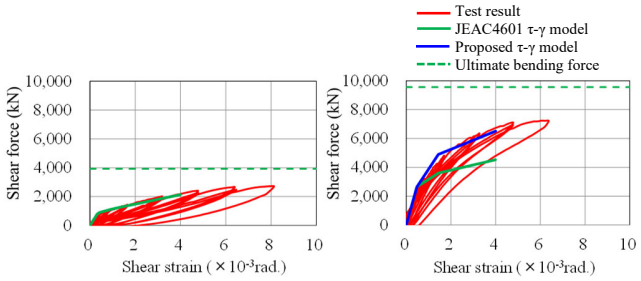

(a) No.1 (b) No.2

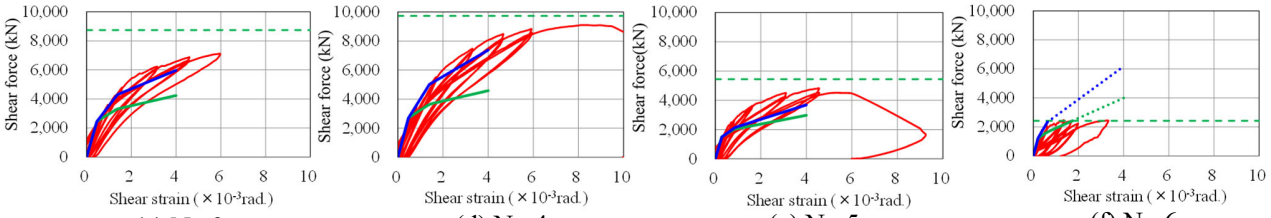

(c) No.3 (d) No.4 (e) No.5 (f) No.6

Figure4.3.2. The comparison of proposed restoring force characteristics to the test results

(2) Moment-Curvature (M-φ) Model

Figure 4.3.3 shows moment-curvature relations of No.2 and No.4 results. After the development of cracks, the stiffness of specimen No.4 is higher than that of specimen No.2, which indicates that the moment resistance was increased due to the steel fiber-reinforcement effects. The moment-curvature model adapts Bernoulli-Euler hypothesis same as JEAC method. For specimens with steel fiber-reinforcement, as shown in Figure 4.3.4, the tensile resistance of steel fibers (5.5N/mm^2) is added to the secondary turning point (yield point) but not to the ultimate strength because the cross-linking effect of the steel fiber is no more expected at the final stage. The model 2 is usually used for a section with steel fiber-reinforcement, but when the specimen is jointed at the bottom of the wall as in this test, the specimen yields at the section without steel fiber-reinforcement, and thus the test results for specimen No.6 is evaluated by model 3.

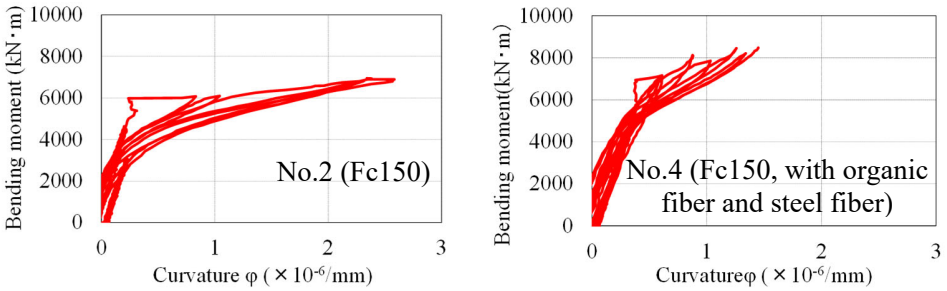

Figure 4.3.3. The comparison of bending moment- curvature relations of No.2 and No.4

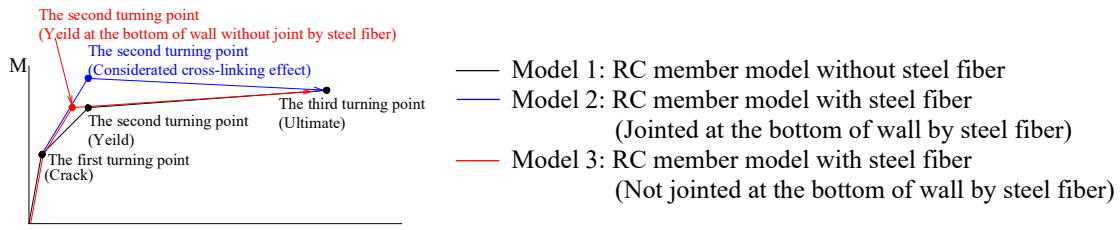

Figure 4.3.4. An image of M-φ model

5. SEISMIC RESPONSE ANALYSIS

Targeting a typical PWR nuclear power plant, seismic response analyses are performed for MDOF (Multiple Degree of Freedom) lumped mass stick models using conventional material (hereinafter referred to as conventional material model) and a model to which restoring characteristics proposed above applied (hereinafter referred to as new material model). The input ground motion and the scope of high-performance concrete[4)] in the analysis model are shown in Figure 5.1 and Figure 5.2, respectively.
The comparisons of wall and reinforcement bar amount ratios, natural periods, ground contact ratio, the maximum response shear strain, the acceleration response spectra, and the shear response results plotted on skeleton curve between the conventional material model and the new material model are shown in Table 5.1, Table 5.2, Table 5.3, Figure 5.3, Figure 5.4, and Figure 5.5, respectively. The natural periods and acceleration response spectra of the new material model indicates slight tendency of increase in its stiffness, but the peak values of the acceleration response spectra showed little difference between models. In addition, the maximum contact ratios for both the models also showed similar results. Focusing on the building wall bottom where the maximum stress occurs, the required amount of wall for new material model is reduced to 0.7 times that of conventional material model in average, whereas shear strain is reduced to 0.4 times and bending curvature to 0.9 in average, respectively; this could be the result of increased strength due to the application of high performance concrete and the decreased seismic force by the reduction of building weight due to the rationalization of member size.

Table 5.1. The amount ratios of Wall and reinforcement bar

Typical part for seismic evaluation		New material model / Conventional material model	
		Wall amount ratios	Reinforcement bar amount ratios
PCCV	Dome	0.7	0.7
	Cylinder	0.7	0.7
REB	FHB	0.7	1.0
	Outer wall	0.7	0.7
I/C	Seismic resistance wall	1.0	1.0
	Primary/Secondary shield wall	0.7	0.7
	Bottom of PRZ	0.6	0.6

PCCV: Pre-stress concrete containment vessel, REB: Reactor encloser building
I/C: Inner concrete, FHB: Fuel handling building, PRZ: Pressurizer

Table 5.2. Natural periods

Degree	Natural period (s)	
	Conventional material model	New material model
1	0.488	0.488
2	0.284	0.248
3	0.191	0.160
4	0.127	0.112
5	0.104	0.096

Table 5.3. The minimum ground contact ratios

Analysis model	Minimum ground contact ratios (%)
Conventional material model	92.1
New material model	92.8

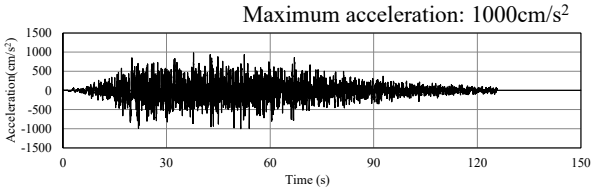

Figure5.1. The waveform of input ground motion

A. UHPC with organic fiber and steel fiber (Fc150)
B. UHPC with organic fiber (Fc100)
C. Normal concrete (Fc33)
D. Heavy weight concrete (Fc33 ~ Fc60)

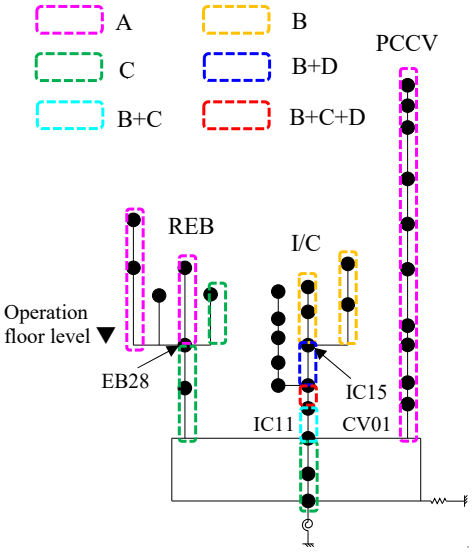

Figure5.2. The analysis model

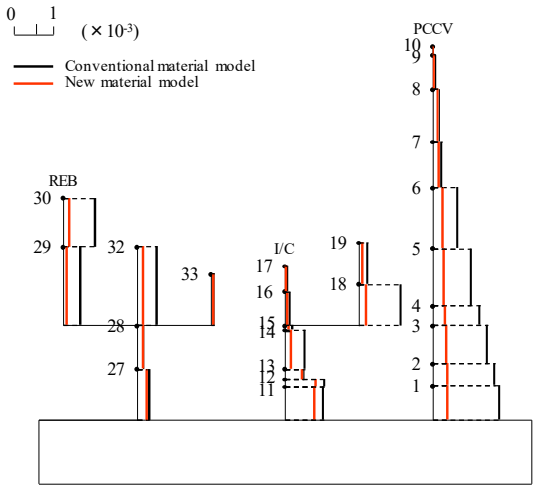

Figure5.3. The maximum response shear strain

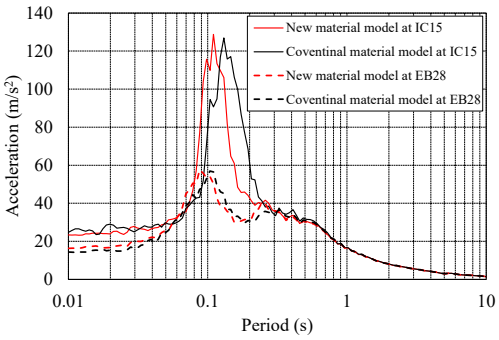

Figure5.4. Acceleration response spectra

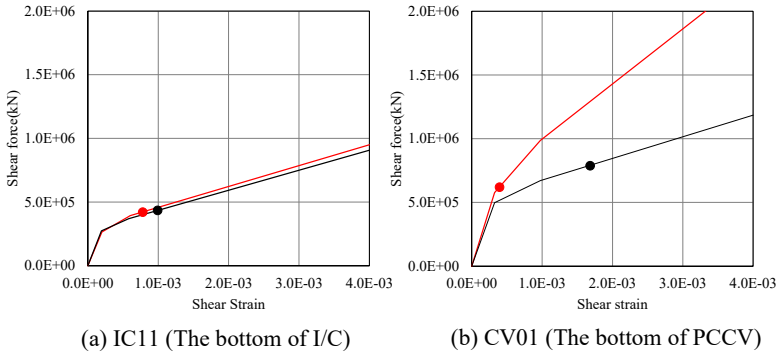

(a) IC11 (The bottom of I/C) (b) CV01 (The bottom of PCCV)

Figure5.5. The shear response results

6. CONCLUSION

A series of loading tests was conducted for structural walls using high-performance concrete, fiber-reinforced concrete and heavyweight concrete. From the test results, the correlation between shear strength and concrete strength, the increase in shear strength and bending strength due to the fiber-reinforcement effect are confirmed; the improvement of seismic safety and the reduction of the amount of materials can be expected by the employment of new materials in structural walls of nuclear power plant facilities.
In addition, restoring force characteristics which is in good accordance with dynamic characteristics of high performance concrete obtained from test results are proposed, and from the results of seismic response analysis for PWR reactor building using this proposed characteristics, it is confirmed that the seismic safety is improved by the increase in structural wall strength and the decrease in seismic force due to the rationalization of member size.

ACKNOWLEDGEMENT

This study had been caried out in “the project on development of technical basis for improving nuclear safety”. funded by Ministry of Economy, Trade and Industry (METI).

REFERENCES

1) The Japan Electric Association (2015). “Technical Code for Seismic Design of Nuclear Power Plants (JEAC 4601-2015)”
2) Nishioka, Y., Tokunaga, M., Tanabe, Y., Shimizu, Y., Nakayama, Y. and Hagiwara, R. (2018). “Study on concrete materials, structure and construction method for nuclear power plant building. Part5 Basic characteristics test result of new materials used for nuclear power building (high strength concrete and high strength steel fiber reinforced concrete)”, *Summaries of Technical Papers of Annual Meeting, Architectural Institute of Japan*, 1135-1136
3) Takami, S, Yukawa, M., Nagashima, G., Nakayama, Y., Hagiwara, R., Takeuch, Y., Tanabe, Y. and Hirotani, T. (2019). “Study on concrete materials, structure and construction method for nuclear power plant building. Part23 Loading test of shear wall using high strength concrete (Restoring Force Model for Structural Design)”, *Summaries of Technical Papers of Annual Meeting, Architectural Institute of Japan*, 1135-1136
4) Nagashima, G., Yamamoto, T., Morita, K., Hagiwara, R. (2022): “FEASIBILITY ASSESSMENT OF ULTRA-HIGH-PERFORMANCE-CONCRETE APPLICATION TO NPPs”, SMiRT 26, Germany, July